Available online at www.sciencedirect.com
SCIENCE DIRECT®
Journal of Molecular Catalysis A: Chemical 218 (2004) 217–227
JOURNAL OF MOLECULAR CATALYSIS A: CHEMICAL
www.elsevier.com/locate/molcata

Density functional theory studies of acetylene hydrogenation on clean, vinylidene- and ethylidyne-covered Pt(1 1 1) surfaces

Simon G. Podkolzin[1], Rafael Alcalá, James A. Dumesic*

Department of Chemical Engineering, University of Wisconsin, Madison, WI 53706, USA

Received 11 December 2003; received in revised form 8 April 2004; accepted 8 April 2004

Abstract

Density functional theory (DFT) calculations for acetylene hydrogenation on clean, vinylidene CCH_2-covered (0.25 ML) and ethylidyne CCH_3-covered (0.25 ML) Pt(1 1 1) surfaces were performed to probe the reaction mechanism and evaluate energetic changes due to high hydrocarbon coverage. A comparison between the reaction energetics on the clean and pre-covered surfaces shows that high coverage trends are similar for vinylidene and ethylidyne species: surface hydrocarbon species and hydrogen are destabilized by up to 150 and 30 kJ/mol, respectively. Unsaturated, multiply-bonded species are destabilized more than species forming fewer bonds with the surface. Activation energies are not affected, unless the spatial formation of a transition state is hindered or a reactant is significantly distorted. In these cases, activation barriers can be different by up to 50 kJ/mol and the relative significance of parallel steps may change. For example, CH_2CH_2 formation is hindered at high coverage and the relative propensity of $CHCH_2$ for forming either CH_2CH_2 or $CHCH_3$ is reversed. The calculations confirm that vinylidene CCH_2 and ethylidyne CCH_3 are spectator species in the overall reactions of ethylene and ethane formation. However, at the evaluated surface coverage of 0.25 ML, these spectator species may undergo hydrogen disproportionation with other hydrocarbon fragments, serving as a hydrogen reservoir and providing lower-energy pathways. As a result, the predicted energetics for acetylene hydrogenation at high coverage are affected by not only the extent of destabilization of active species and their transition states, but also by the relative stability of spectator species and their possible participation in disproportionation reactions.

Keywords: Hydrogen; Acetylene; Ethylene; Ethane; Vinylidene; Ethylidyne; Hydrogenation; Adsorption; Platinum; Lateral interactions; DFT; Spectator species

1. Introduction and background

Selective hydrogenation of unsaturated hydrocarbons and, specifically, selective hydrogenation of acetylene to ethylene, is widely used in the petroleum and chemical industries. Commercial catalysts are predominantly based on alumina-supported Pd-based alloys. In the present study, however, we have chosen to study acetylene hydrogenation on platinum because of the availability of experimental and theoretical surface science data on the stability and reactivity of C_2 hydrocarbons on this metal. We note in this respect that most surface science results, both theoretical and experimental, are obtained at low surface coverages, whereas hydrogenation reactions, which are usually run at temperatures below 400 K, proceed over highly covered catalytic surfaces. As a result, one of the challenges in understanding the kinetics of these reactions is bridging the gap between results of surface science studies usually conducted at low coverage conditions and results of reaction kinetic studies typically conducted at high coverage.

The most abundant surface species under typical reaction conditions are hydrocarbon spectator species, which do not contribute appreciably to the overall hydrogenation rate [1–7]. In this work, we consider two of the most stable acetylene-derived spectator species: vinylidene CCH_2 and ethylidyne CCH_3 species. The objective of our study is to identify and evaluate trends caused by the presence of these spectator species on the energetics of reactive intermediates

* Corresponding author. Tel.: +1-608-262-1095; fax: +1-608-262-5434.
E-mail address: dumesic@engr.wisc.edu (J.A. Dumesic).
[1] Present address: The Dow Chemical Company, Core Research and Development, Midland, MI 48674, USA.

1381-1169/$ – see front matter © 2004 Elsevier B.V. All rights reserved.
doi:10.1016/j.molcata.2004.04.015

for acetylene hydrogenation on Pt(1 1 1). We extend our previously reported results for C_2 species on Pt(1 1 1) in the low-coverage limit [8–10] to calculations at a near saturation coverage. A highly covered surface model is generated by using a periodic slab with a small unit cell and by adding a hydrocarbon spectator species to this cell.

A summary of early reaction kinetics results for acetylene hydrogenation over Pt can be found in reviews by Bond and Wells [11] and Webb [12]. A review of more recent kinetic studies has been published by Bos and Westerterp [13]. The chemistry of C_2 hydrocarbon species on Pt surfaces has been reviewed by Zaera and coworkers [14–17].

2. Methods

Density functional theory (DFT) calculations were performed with the DACAPO software from the Technical University of Denmark [18]. An infinite Pt(1 1 1) slab model constructed from a 2×2 unit cell with two metal layers was used in self-consistent periodic-slab calculations based on gradient-corrected density functional theory (DFT-GGA). The two metal layers were separated by four equivalent layers of vacuum. Ionic cores were described by ultrasoft pseudopotentials, and the Kohn–Sham one-electron valence states were expanded in a basis of plane waves with kinetic energies below 25 Ry. The surface Brillouin zone was sampled at a specified number of *k*-points. Initial geometries were generated using sampling at 6 *k*-points, and then the structures were re-optimized with 18 *k*-points. The exchange-correlation energy and potential were described by the generalized gradient approximation (PW-91). The self-consistent PW-91 density was determined by iterative diagonalization of the Kohn–Sham Hamiltonian, Fermi-population of the Kohn–Sham states ($k_B T = 0.1$ eV), and Pulay mixing of the resulting electronic density. All reported binding energies were extrapolated to $k_B T = 0$ eV.

The positions of the Pt(1 1 1) slab atoms were constrained during the calculations at values corresponding to the lattice constant of 4.00 Å [8]. Adsorbates were allowed to optimize fully. Gas-phase calculations were carried out with a 15 Å unit cell. Transition state geometries were estimated with constrained optimization calculations, in which a bond length, in this case the C–H bond distance, was constrained and all other degrees of freedom were optimized. A transition state was identified as a configuration having the maximum energy along the C–H bond extension coordinate and characterized by a transition from attractive to repulsive forces for the constrained bond.

State-of-the-art DFT slab calculations use multiple layers, allowing the top one or more layers to relax during optimization to account for surface relaxation. Our DFT calculations indicate that the combined effect of increasing the slab thickness to three layers and relaxing the first metal layer stabilizes hydrocarbon surface species by about 20 kJ/mol [8]. The fixed-slab calculations used in the current study do not evaluate this effect because the primary objective of this paper is to identify energetic trends due to high surface coverage. These trends were evaluated by comparing results for adsorption and hydrogenation on a 2×2 unit cells (reactive hydrocarbon coverage 0.25 ML) with results for the same reactions in the presence of a spectator species in the same unit cell (total hydrocarbon coverage 0.5 ML). The DFT calculations predict values of gas-phase energy changes for acetylene hydrogenation to ethylene of −220 kJ/mol and for acetylene hydrogenation to ethane of −391 kJ/mol. The values based on the enthalpies of formation at 25 °C are, correspondingly, −174 and −311 kJ/mol [19]. The differences between the theoretical and experimental values are partially due to neglect of zero-point energy (ZPE) corrections [20] and also to limitations of DFT calculations. Corrections can be introduced to reconcile thermodynamics of surface species [21]. In this study, however, where the relative stabilities and reactivities of surface species are evaluated at different coverage values, the effects of surface relaxation, ZPE and temperature corrections are not critical because they should substantially cancel out in the calculation of relative energetic trends.

In high coverage calculations, both a reactive hydrocarbon and a spectator species, either ethylidyne CCH_3 or vinylidene CCH_2, were fully optimized. An additional complexity for configurations with vinylidene CCH_2 spectator species was its stability in three different geometries: leaning over a three-fold site from a bridge site ($\mu_3 - \eta^2$), orthogonal on a bridge site ($\mu_2 - \eta^1$), and orthogonal on a three-fold site ($\mu_3 - \eta^1$) (μ denotes the number of bonds with the surface, and η the number of bonding carbon atoms). As a result, for most configurations, all three conformations were evaluated separately to find the most favorable one. We note that only the first two vinylidene geometries: CCH_2 $\mu_3 - \eta^2$ and $\mu_2 - \eta^1$ are stable on the clean surface. The third geometry, CCH_2 $\mu_3 - \eta^1$, becomes favorable only at high coverage.

Energy diagrams were constructed with the following reference state: $C_2H_2(gas) + 2H_2(gas) + 5Pt$, where Pt denotes a model slab that is either clean, vinylidene- or ethylidyne-covered Pt(1 1 1). The first reaction step is dissociation and adsorption of the two hydrogen molecules, so that the system becomes $C_2H_2(gas) + Pt + 4H^*$. The second step is acetylene adsorption. Subsequently, the reaction proceeds through transfer of one surface H onto the slab with the surface acetylene, followed by addition of the first H atom to adsorbed acetylene. The hydrogenation proceeds further by a similar consecutive transfer and reaction of the remaining 3H atoms. Activation energies for forward reactions are quoted based on the configurations where the reactant hydrocarbon and hydrogen are on separate slabs, i.e., the activation energies include barriers for bringing a hydrogen atom from another lattice into the unit cell with the hydrocarbon.

3. Stable species on Pt(1 1 1)

A list of evaluated hydrogen and C_2 hydrocarbon species on clean Pt(1 1 1) is provided in Table 1. Only the most stable identified configuration is shown for each species, except for vinylidene. The energy values in Table 1 are quoted with respect to the gas-phase reference state of C_2H_2 plus $2H_2$, with hydrogen molecules adsorbed first as H atoms. For example, the energy for the acetylene geometry in entry 2 in Table 1 is computed by summing the adsorption energy for $4H^*$, entry 1 in Table 1, and the acetylene adsorption energy: -172 to $219 = -391$.

The adsorption energy for dissociative adsorption of molecular hydrogen in an fcc site (three-fold site without a Pt atom below it in the second layer) is -86 kJ/mol. This number is in agreement with experimental results and previously reported theoretical values [9]. The hydrogen adsorption energies for other high symmetry sites are similar, i.e., hcp (three-fold site with a Pt atom below it in the second layer), atop, and bridge sites. The most stable acetylene adsorption mode is the $\mu_3 - \eta^2$ surface species in an hcp site. The calculated adsorption energy for this structure is -219 kJ/mol, entry 13 in Table 1. This value is in agreement with the heat of acetylene adsorption of -210 kJ/mol obtained by microcalorimetric measurements on Pt powder at 173 K [22]. Previous DFT calculations with a Pt_{10} cluster predicted a similar geometry with a comparable heat of adsorption of -212 kJ/mol [23]. A recent plane-wave calculation with a periodic Pt slab identified the same geometry with a heat of adsorption of -229 kJ/mol [24]. In contrast, a higher adsorption energy of -330 kJ/mol was reported based on calculations with a Pt_8 cluster [21], which is probably due to the sensitivity of results to the size and shape of the cluster. In our identified acetylene configuration, the C–C bond is parallel to the surface, and the bond length is 1.40 Å. This distance is in agreement with values of 1.35–1.39 Å obtained from spectroscopic studies [25]. This di-σ–π-adsorption mode was proposed for Pt(1 1 1) based on vibration spectra and for Pd(1 1 1) based on photoelectron diffraction studies and Hartree–Fock cluster calculations [26–28]. This geometry, with the C–C bond axis being parallel to the surface, is also consistent with the interpretation of angle resolved photoemission data for Pt(1 1 1) [29].

Table 1
Energetics of stable species on Pt(1 1 1), kJ/mol

	Species	Pt(1 1 1)
1	$4H^*$ (fcc) + C_2H_2 gas	−172
2	$CHCH^*$ $\mu_3 - \eta^2$ (hcp) + $4H^*$	−391
3	CCH_2^* $\mu_3 - \eta^2$ + $4H^*$	−404
4	CCH_2^* $\mu_2 - \eta^1$ + $4H^*$	−332
5	$CHCH_2^*$ $\mu_3 - \eta^2$ (fcc) + $3H^*$	−399
6	CCH_3^* $\mu_3 - \eta^1$ (fcc) + $3H^*$	−460
7	$CH_2CH_2^*$ $\mu_2 - \eta^2$ (di-σ-bonded) + $2H^*$	−405
8	$CHCH_3^*$ $\mu_2 - \eta^1$ (bridge) + $2H^*$	−371
9	C_2H_4 gas + $2H^*$	−306
10	$C_2H_5^*$ $\mu_1 - \eta^1$ (atop) + H^*	−385
11	C_2H_6 gas	−391
12	$H_2 + 2^* = 2H^*$	−86
13	$C_2H_2 + * = CHCH^*$	−219
14	$C_2H_4 + * = CH_2CH_2^*$	−99

Reference state: C_2H_2(gas) + $2H_2$(gas) + Pt(1 1 1) for steps 1–11, and Pt(1 1 1) plus gaseous adsorbate for steps 12–14.

The formation of vinylidene CCH_2 species on Pt(1 1 1) at temperatures near 300 K has been identified in spectroscopic and electron diffraction studies [30–32]. NMR results suggest that the ratio of acetylene to vinylidene on highly dispersed Pt particles is 1:4 [33]. We considered two vinylidene adsorption modes: one in a three-fold site in a leaning position at a 40° angle with a C–C bond length of 1.41 Å, entry 3 in Table 1, and the other on a bridge site in a position orthogonal to the surface with a C–C bond length of 1.34 Å, entry 4 in Table 1. Both vinylidene configurations were observed spectroscopically on thermal evolution of acetylene from Pt(1 1 1) [32,34]. The energetics of a leaning CCH_2 $\mu_3 - \eta^2$ in fcc and hcp sites are similar. This configuration is the most stable for the C_2H_2 stoichiometry, corresponding to an acetylene adsorption energy of -232 kJ/mol. These results are in agreement with previously reported values for a Pt_{10} cluster [23]. A significantly different value of -404 kJ/mol was reported for CCH_2 in a three-fold site of a Pt_8 cluster [21]. The orthogonal $\mu_2 - \eta^1$ configuration of vinylidene CCH_2, entry 4 in Table 1, is less stable by 72 kJ/mol compared to the $\mu_3 - \eta^2$ species. In spite of this energetic difference, this CCH_2 configuration is more geometrically compact, making it preferable at high coverage, according to results presented below.

Ethylene adsorption on Pt surfaces has been extensively studied by theoretical methods, e.g., [21,35–40]. Ethylene can adsorb as a di-σ-bonded species on a bridge site (adsorption energy of -99 kJ/mol, entries 7 and 14 in Table 1) or as π-bonded species on an atop site (-68 kJ/mol, not shown in tables). The optimized geometries were similar to the ones reported for Pt(1 1 1), Pt_{19} and Pt_{10} [8,23,41]. The estimated adsorption energies are consistent with experimental values. Specifically, the adsorption enthalpy for di-σ-bonded species was found to be -124 kJ/mol on Pt(1 1 1) with collision-induced desorption (CID) [42] and -136 kJ/mol on Pt(1 1 0)(2 × 1) with adsorption calorimetry [43]. Calorimetric measurements for ethylene adsorption yielded values of -120 kJ/mol for Pt powder [22] and -125 kJ/mol for Pt/SiO_2 [41] under conditions where predominantly di-σ-bonded species were formed. The adsorption enthalpy for π-bonded species was reported to be -40 ± 10 kJ/mol based on reflection–adsorption infrared spectroscopy (RAIRS) [44] and -92 kJ/mol based on CID with oxygen precovered Pt(1 1 1) [45]. Recent molecular beam results show that di-σ- and π-bonded species have different adsorption kinetics, with the π-bonded species being adsorbed more weakly and reversibly on a hydrocarbon covered surface [46]. In addition, isotope experiments indicate that the interconversion between these two species

is relatively slow compared to ethylene adsorption rates [46].

In agreement with experimental evidence and numerous theoretical studies, our calculations confirm that it is thermodynamically favorable for surface ethylene to rearrange with the formation of ethylidyne CCH_3, entry 6 in Table 1, and surface hydrogen. The predicted energy change for the dissociative ethylene adsorption is −154 kJ/mol, which is consistent with experimental values. Specifically, calorimetric measurements were used to obtain values of −174 ± 4 kJ/mol for Pt(1 1 1) [47], −150 kJ/mol for a Pt film [48], −160 kJ/mol for a Pt powder [22], and −157 to −145 kJ/mol for Pt/SiO_2 [41,49].

The configuration for adsorbed $CHCH_2$ species in a three-fold fcc site, entry 5 in Table 1, is less stable than ethylidyne by 61 kJ/mol, which is in agreement with reported theoretical values of 53–70 kJ/mol [8,21]. The configuration of $CHCH_3$ species in a bridge site, entry 8 in Table 1, is less stable than di-σ-bonded ethylene by 34 kJ/mol, which is consistent with reported values of 34–44 kJ/mol [8,21]. The methyl group of $CHCH_3$ is orthogonal to the two bonding Pt atoms, and its rotation is energetically unfavorable. In contrast, the C_2H_5 species on an atop site, entry 10 in Table 1, has an unhindered methyl rotation, allowing this species to maintain its favorable configuration at high coverage.

4. Transition states on Pt(1 1 1)

A summary of transition state energetics for Pt(1 1 1) is provided in the first column of Table 2a. The corresponding activation barriers for forward reactions are provided in Table 2b. The geometries of the transition states are schematically shown in Fig. 1. The calculated energetic penalty for adding an H into the lattice unit cell, which is occupied by one hydrocarbon species, is 30–40 kJ/mol. Accordingly, all our intrinsic activation barriers are higher than this number. The estimated barriers for forward hydrogenation reactions range from 67 to 143 kJ/mol. Experimental values for the apparent activation energy over Pt catalysts range from 40 to 70 kJ/mol [11,12]. The apparent activation energies are generally lower because they represent a combined effect of stabilization of reacting species on the catalytic surface and intrinsic barriers for conversion of reacting adsorbates.

Table 2
Energetics of transition states and activation energies for reactions with surface H (kJ/mol)

	Reaction	Pt	Pt-CCH_2	Pt-CCH_3
(a) Energetics of transition states				
1	$CHCH + H = CHCH_2$	−304	−138	−127
2	$CCH_2 + H = CCH_3$	−313	−162	
3	$CHCH_2 + H = CH_2CH_2$	−332	−150	−151
4	$CHCH_2 + H = CHCH_3$	−319	−182	−157
5	$CCH_3 + H = CHCH_3$	−317		
6	$CH_2CH_2 + H = C_2H_5$	−291	−158	−116
7	$CHCH_3 + H = C_2H_5$	−282	−113	−107
(b) Activation energies				
1	$CHCH + H = CHCH_2$	87	85	96
2	$CCH_2 + H = CCH_3$	91	98	
3	$CHCH_2 + H = CH_2CH_2$	67	111	101
4	$CHCH_2 + H = CHCH_3$	80	79	95
5	$CCH_3 + H = CHCH_3$	143		
6	$CH_2CH_2 + H = C_2H_5$	114	80	106
7	$CHCH_3 + H = C_2H_5$	89	103	101

Reference state: C_2H_2(gas) + $2H_2$(gas) + Pt(1 1 1) (clean, CCH_2 or CCH_3-covered).

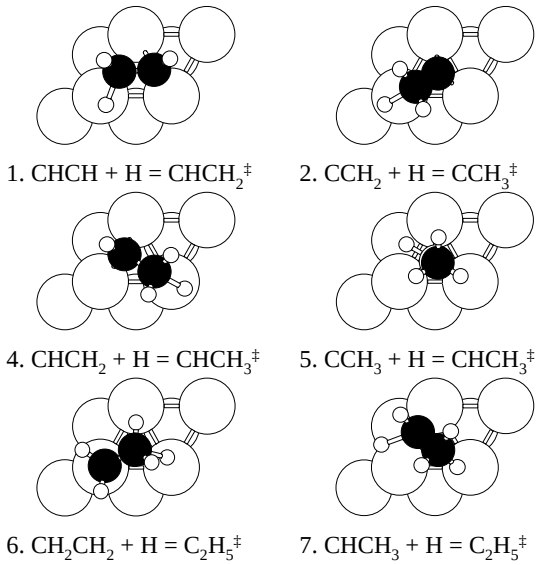

Fig. 1. Geometries of transition states on Pt(1 1 1). Numbers correspond to reactions in Table 2. Reaction 3 in Table 2 is shown in Fig. 2a.

The activation barriers for hydrogenation of acetylene and vinylidene CCH_2 (forming $CHCH_2$ and ethylidyne CCH_3, respectively) are similar, equal to 87 and 91 kJ/mol (reactions 1 and 2 in Table 2b). Recent RAIRS and TPD studies with deuterated ethylene and diodoethane on Pt(1 1 1) suggest that ethylidyne formation proceeds through a $CHCH_3$ intermediate and that the formation kinetics are coverage dependent due to a lack of vacant sites required for splitting hydrogen at high coverage [50,51]. This pathway for ethylidyne formation was not evaluated in the current study since acetylene is assumed to be the main source for all hydrocarbon surface species.

The transition state energy for ethylidyne hydrogenation is approximately the same (−317 kJ/mol) as that for hydrogenation of $CHCH_2$ to form $CHCH_3$ (−319 kJ/mol), as shown in Table 2a. The transition state energy (−332 kJ/mol) for forming ethylene from $CHCH_2$ is lower by about 15 kJ/mol. Two evaluated pathways for this transition state are presented in Fig. 2. In the first scenario in Fig. 2a, a hydrogen atom moves across the unit cell, following the $CHCH_2$ species, to form a di-σ-bonded ethylene species. The estimated activation barrier for this pathway is 67 kJ/mol, reaction 3 in Table 2b. In contrast, the barrier is higher by 81 kJ/mol for the transition state formed when the hydrocarbon species and hydrogen move toward each

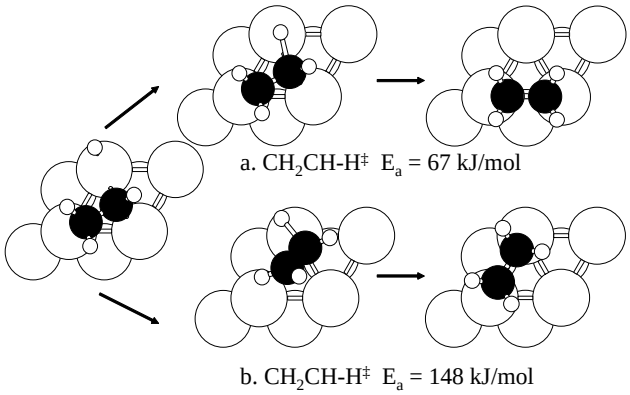

Fig. 2. Two scenarios for forming di-σ-ethylene: (a) hydrogen follows the hydrocarbon across the unit cell—this pathway is preferable on a clean surface; (b) hydrogen and hydrocarbon move toward each other—this pathway becomes preferable at high hydrocarbon coverage.

other, as shown in Fig. 2b. The first pathway, however, becomes unfeasible in the presence of a spectator species. Implications of this geometric restriction will be discussed below with respect to the vinylidene-covered surface.

With regard to the reactivity of vinylidene and ethylidyne species, which are usually treated as spectators in hydrogenation, we note that the formation of ethylidyne species from vinylidene has a barrier of 91 kJ/mol, reaction 2 in Table 2b, which is lower than the barrier of 112 kJ/mol for the formation of $CHCH_2$ species (not shown in the tables). In addition, the activation energy for ethylidyne hydrogenation of 143 kJ/mol is significantly higher than the barriers of all other species, and ethylidyne can be considered inactive in the presence of another hydrocarbon species. As a result, our calculations confirm that reactions of vinylidene and ethylidyne species with surface hydrogen are not expected to contribute measurably to the overall hydrogenation rate.

The calculated barrier for the hydrogenation of di-σ-bonded ethylene is 114 kJ/mol. The corresponding transition state is shown in Fig. 1(6). The C–H distance in our transition state is 1.7 Å, which is in agreement with the value in a recent DFT study with a Pt_{10} cluster [39]. Furthermore, this study reports an activation energy of 81 kJ/mol for di-σ-bonded ethylene from the reference state where the hydrocarbon and hydrogen are on the same cluster. A comparative number from our calculations is 89 kJ/mol for the reference state of di-σ-bonded ethylene and hydrogen in the same unit cell, with the unconstrained C–H distance being 3.1 Å.

Spectroscopic studies and molecular beam experiments suggest that the hydrogenation rate of ethylene in the π-bonded configuration is higher than that of the di-σ-bonded species [52,53]. In our calculations, the relative hydrogenation activities for the two ethylene surface species could not be evaluated due to limitations of the constrained optimization method employed in the estimation of activation energies. The barrier for the transition between π- and di-σ-bonded ethylene is small compared to that for the hydrogen addition step, and therefore, the identified transition state in Fig. 1(6) could not be linked unambiguously to one of the surface ethylene configurations. As a result, the activation energies for reaction 6 in Table 2b and also in Fig. 5 are quoted with respect to the most stable species, di-σ-bonded ethylene. A DFT study with a Pt_{10} cluster showed that di-σ-bonded ethylene was more reactive [39]. The apparent discrepancy with experimental evidence was attributed to the fact that the barriers were estimated at low coverage. In a DFT study with Pd(1 1 1) model surfaces, π-bonded ethylene was found to rearrange into di-σ-bonded species prior to hydrogen addition at low coverage [54]. In contrast, at 0.6 ML in the presence of surface hydrogen, ethylene was reported to be pinned in the π-bonded configuration due to repulsive lateral interactions [54].

The transition state for $CHCH_3$ hydrogenation is shown in Fig. 1(7). The barrier for this step is about 25 kJ/mol lower than that for ethylene hydrogenation, reactions 6 and 7 in Table 2. Further hydrogenation of C_2H_5 and formation of gas-phase ethane were not evaluated because ethylene and hydrogen co-adsorption measurements and experiments with ethyliodide showed that the C_2H_5 hydrogenation step is facile, with an estimated activation energy of only 25 kJ/mol [55–58]. Consequently, this step was not expected to influence the overall apparent reaction energetics.

5. Stable species on Pt(1 1 1)-CCH_2

A summary of energetics for stable species on the vinylidene-covered surface is provided in Table 3. The corresponding geometries are shown in Fig. 3. The most favorable location for a hydrogen atom in the presence of vinylidene is on the atop site of the metal atom that

Table 3
Energetics of stable species on vinylidene CCH_2-covered surface (kJ/mol)

	Species	Pt(1 1 1)-CCH_2
1	$CCH_2^* \ \mu_3 - \eta^2 - 4H^* \ \mu_1$ (atop) + C_2H_2 gas	−147
2	$CCH_2^* \ \mu_3 - \eta^2 - CCH_2^* \ \mu_3 - \eta^1 + 4H^*$	−260
3	$CCH_2^* \ \mu_2 - \eta^1 - CHCH^* \ \mu_3 - \eta^2$ (fcc) + $4H^*$	−223
4	$CCH_2^* \ \mu_2 - \eta^1 - CHCH_2^* \ \mu_3 - \eta^2 + 3H^*$	−261
5	$CCH_2^* \ \mu_2 - \eta^1 - CCH_3^* \ \mu_3 - \eta^{1*} + 3H^*$	−316
6	$CHCH^* \ \mu_3 - \eta^2$ (hcp) − $CCH_3^* \ \mu_3 - \eta^1 + 3H^*$	−320
7	$CCH_2^* \ \mu_2 - \eta^1 - CH_2CH_2^* \ \mu_2 - \eta^2$ (di-σ-bonded) + $2H^*$	−238
8	$CCH_2^* \ \mu_2 - \eta^1 - CHCH_3^* \ \mu_2 - \eta^1$ (bridge) + $2H^*$	−216
9	$CCH_2^* \ \mu_3 - \eta^2 + C_2H_4$ gas + $2H^*$	−294
10	$CCH_2^* \ \mu_3 - \eta^2 - C_2H_5^* \ \mu_1 - \eta^1$ (atop) + H^*	−277
11	$CCH_2^* \ \mu_3 - \eta^2 + C_2H_6$ gas	−391
12	$H_2 + 2^* = 2H^*$	−73
13	$C_2H_2 + * = CHCH^*$	−76
14	$C_2H_4 + * = CH_2CH_2^*$	56

Reference state: C_2H_2(gas) + $2H_2$(gas) + Pt(1 1 1)-CCH_2 for steps 1–11, and Pt(1 1 1)-CCH_2 plus gaseous adsorbate for steps 12–14.

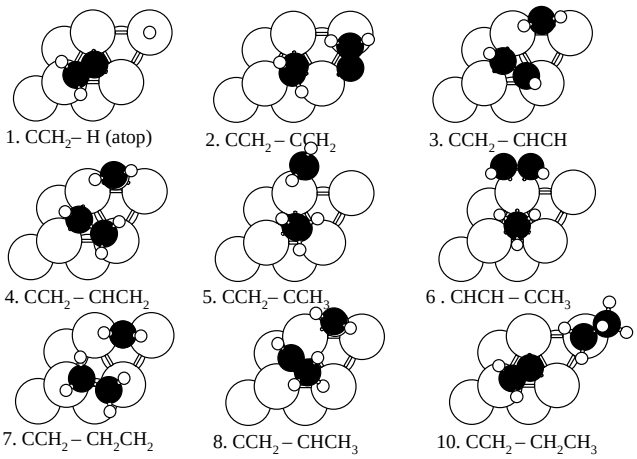

Fig. 3. Geometries of stable species on vinylidene CCH_2-covered Pt(1 1 1) surface. Numbers correspond to entries in Table 3. Entry 9 is not shown: CCH_2 $\mu_3-\eta^2$ plus gas-phase ethylene.

is not associated with the hydrocarbon, Fig. 3(1). The energy change for dissociative adsorption is estimated at −73 kJ/mol, entry 12 in Table 3. The presence of vinylidene makes H_2 adsorption less exothermic by 13 kJ/mol.

The optimized configuration for acetylene adsorption on the vinylidene-covered surface is shown in Fig. 3(3). It is energetically favorable for vinylidene to rearrange from CCH_2 $\mu_3-\eta^2$ to $\mu_2-\eta^1$, incurring a penalty of 72 kJ/mol (difference between these two modes on the clean surface, entries 3 and 4 in Table 1) but providing sufficient space for acetylene stabilization. The energy of the optimized configuration corresponds to the energy of acetylene adsorption on a vinylidene-covered surface of −76 kJ/mol, entry 13 in Table 3. The most stable adsorption mode for this stoichiometry (i.e., four carbon and four hydrogen atoms in the same unit cell) is adsorption of two vinylidene species, Fig. 3(2) and entry 2 in Table 3. In this arrangement, both vinylidene species are associated with three metal atoms, the μ_3-configuration. Although one of them is similar to the leaning CCH_2 $\mu_3-\eta^2$ on the clean surface, the other one is a distorted version of the orthogonal CCH_2 $\mu_2-\eta^1$ species. The distorted species is tilted and bonded to three metal atoms on a three-fold site.

The di-σ-ethylene adsorption mode becomes distorted on the vinylidene-covered surface, Fig. 3(7), and resembles the structure favored based on low energy electron diffraction (LEED) results at high coverage [59]. The predicted energy change for ethylene adsorption is 56 kJ/mol (endothermic), entry 14 in Table 3. This destabilization suggests that ethylene should desorb readily in the presence of a hydrocarbon overlayer. As mentioned above, molecular beam experiments indicate that at high coverage, ethylene adsorbs reversibly as π-bonded species that can transform into the di-σ-configuration [46] with an estimated adsorption energy of −46 kJ/mol [58]. Our calculations for π-bonded ethylene show that the geometry of this species is practically unaffected by the presence of vinylidene. Accordingly, π-bonded ethylene is estimated to be less stable than di-σ-bonded species by 31 kJ/mol on the clean surface and only by 6 kJ/mol in the presence of vinylidene (not shown in tables). Similar to π-bonded ethylene, the geometries of $CHCH_3$ and C_2H_5 species (Fig. 3(8) and (10), respectively) on the vinylidene-covered surface are analogous to those on the clean surface.

6. Transition states on Pt(1 1 1)-CCH_2

A summary of transition state energetics for a vinylidene-covered surface (Pt-CCH_2) is provided in the second column of Table 2a. The corresponding activation barriers for forward reactions are given in Table 2b. The geometries of the transition states are shown in Fig. 4. The transition state with the lowest energy for the first hydrogenation step corresponds to the reaction of a vinylidene species in the presence of another vinylidene to form ethylidyne, Fig. 4(2). This result is similar to the one on the clean surface and is consistent with the experimental evidence of ethylidyne formation on acetylene adsorption in the presence of hydrogen [26,32,34,60]. The transition state for acetylene hydrogenation in the presence of vinylidene is higher on the energy diagram by 24 kJ/mol, reaction 1 in Table 2a. The starting configuration for this transition state was the acetylene–vinylidene pair in Fig. 3(3). To compare the relative reactivities of vinylidene and acetylene at high coverage, the same configuration in Fig. 3(3) was used to estimate the activation energy for vinylidene hydrogenation. This estimate for vinylidene hydrogenation in the presence of acetylene is 95 kJ/mol (not shown in the tables), which is consistent with the value of 98 kJ/mol obtained in the presence of another vinylidene, reaction 2 in Table 2b. This value is higher than the value of 85 kJ/mol for acetylene hydrogenation, reaction 1 in Table 2b. These results indicate that if both acetylene and vinylidene are present, acetylene is likely to be more reactive for hydrogenation. Furthermore, vinylidene is more likely to form ethylidyne than $CHCH_2$ on hydrogenation and, thus, cannot be expected to

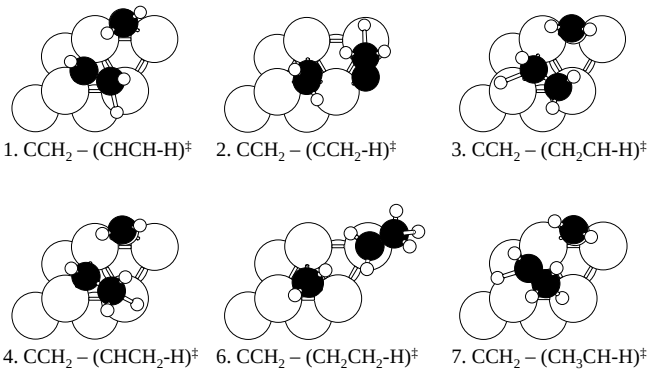

Fig. 4. Geometries of transition states on Pt(1 1 1)-CCH_2. Numbers correspond to reactions in Table 2. Reaction 5 in Table 2, CCH_3 hydrogenation at high coverage, was not evaluated.

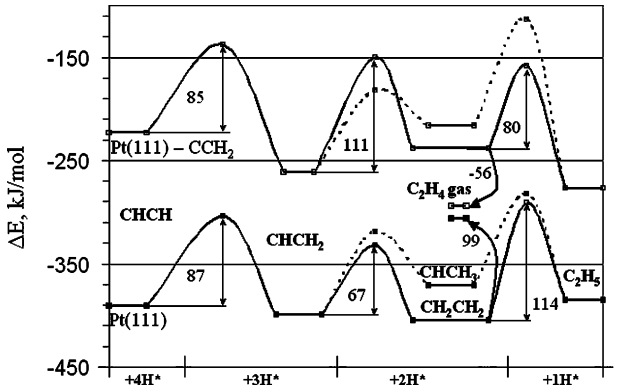

Fig. 5. Comparison of the main features of the acetylene hydrogenation energy diagrams on clean and vinylidene-covered Pt(1 1 1). Reference state: $C_2H_2(gas) + 2H_2(gas) + Pt(1\,1\,1)$ or Pt(1 1 1)-CCH_2. Dashed lines denote formation and hydrogenation of $CHCH_3$.

contribute appreciably to the overall hydrogenation rate, i.e., the calculations support the characterization of vinylidene as a spectator species.

The main features of the energy diagrams for the consecutive acetylene hydrogenation to C_2H_5 on clean and vinylidene-covered Pt(1 1 1) are compared in Fig. 5. The plot for the vinylidene-covered surface is initially shifted up by about 170 kJ/mol. The difference is due mainly to the destabilization of acetylene in the presence of vinylidene by 143 kJ/mol. The rest of the difference is a result of the lower heat of hydrogen adsorption. The first hydrogenation step of forming $CHCH_2$ becomes more exothermic by 30 kJ/mol because acetylene is destabilized more than the product. This trend is in agreement with the calculations for the same reaction step on Pd(1 1 1) where increasing the coverage of reactive species from 0.25 to 0.33 ML increases the heat of reaction by 17 kJ/mol [61].

The barriers for forming and further hydrogenating $CHCH_3$ species are similar on both diagrams (dashed lines in Fig. 5, also in Table 2b). In contrast, the barriers for forming and hydrogenating ethylene are significantly different. Specifically, the activation energy for forming ethylene is higher on the vinylidene-covered surface by 44 kJ/mol. The transition state leading to ethylene formation on the clean surface, as shown in Fig. 2a, requires the whole 2×2 unit cell, and this transformation becomes restricted in the presence of a vinylidene spectator species. Consequently, the resulting transition state in Fig. 4(3) is less stable and resembles the less favorable reaction pathway on the clean surface shown in Fig. 2b. On the other hand, the barrier for ethylene hydrogenation in the presence of vinylidene is lower than that on the clean surface by 34 kJ/mol (Fig. 5 and Table 2b). This value is in accord with the reported difference of 46 kJ/mol between the intrinsic barriers for the hydrogenation of di-σ-bonded ethylene at low coverage and for π-bonded species at 0.6 ML on Pd(1 1 1) [54]. This barrier reduction in our calculations can be mainly attributed to the destabilization of ethylene species at high coverage. The barrier for ethylene hydrogenation was estimated to be 54 kJ/mol based on cumulative experimental evidence for the reactivity of C_2 hydrocarbon species under vacuum [58]. This value is significantly lower than our estimates of 114 and 80 kJ/mol computed for respectively clean and vinylidene-covered surfaces. With respect to this difference, we note the approximate nature of our calculations, which are intended primarily for the evaluation of relative energetic trends caused by high coverage effects. In addition, in the previously mentioned theoretical study with Pd(1 1 1) [54], this barrier was found to be reduced to 36 kJ/mol at 0.6 ML.

The changes in the energy diagrams in the presence of vinylidene are important in the analysis of selectivity to ethylene production. The energy diagram for the clean surface in Fig. 5 suggests that ethane can be produced from ethylene re-adsorption from the gas phase. In contrast, the diagram for the vinylidene-covered surface suggests that any ethylene formed during the reaction would readily desorb, and that re-adsorption would be unfavorable. For our model with a fixed vinylidene coverage, most of the ethane is predicted to be formed through a direct hydrogenation of $CHCH_3$ species that become relatively more stable compared to adsorbed ethylene at high hydrocarbon coverage.

7. Stable species on Pt(1 1 1)-CCH_3

A summary of energetics for stable species on the ethylidyne-covered surface is provided in Table 4. The corresponding geometries are shown in Fig. 6. Some of the geometries are identical for vinylidene- and ethylidyne-covered surfaces, and they are shown in both Tables 3 and 4: entries 5 and 6 in Table 3 correspond to entries 3 and 2 in Table 4. These structures are shown in Fig. 3 for Pt(1 1 1)-CCH_2, but they are omitted from Fig. 6 for Pt(1 1 1)-CCH_3.

Table 4
Energetics of stable species on ethylidyne CCH_3-covered surface (kJ/mol)

	Species	Pt(1 1 1)-CCH_3
1	CCH_3^* $\mu_3 - \eta^1 - 4H^*$ (fcc) + C_2H_2 gas	−108
2	CCH_3^* $\mu_3 - \eta^1 - CHCH^*$ $\mu_3 - \eta^2$ (hcp) + $4H^*$	−223
3	CCH_3^* $\mu_3 - \eta^1 - CCH_2^*$ $\mu_2 - \eta^1 + 4H^*$	−215
4	CCH_3^* $\mu_3 - \eta^1 - CHCH_2^*$ $\mu_3 - \eta^2 + 3H^*$	−252
5	CCH_3^* $\mu_3 - \eta^1 - CCH_3^*$ $\mu_3 - \eta^1 + 3H^*$	−310
6	CCH_3^* $\mu_3 - \eta^1 - CH_2CH_2^*$ $\mu_2 - \eta^2$ (di-σ-bonded) + $2H^*$	−222
7	CCH_3^* $\mu_3 - \eta^1 - CHCH_3^*$ $\mu_2 - \eta^1$ (bridge) + $2H^*$	−208
8	CCH_3^* $\mu_3 - \eta^1 + C_2H_4$ gas + $2H^*$	−274
9	CCH_3^* $\mu_3 - \eta^1 - C_2H_5^*$ $\mu_1 - \eta^1$ (atop) + H^*	−246
10	CCH_3^* $\mu_3 - \eta^1 + C_2H_6$ gas	−391
11	$H_2 + 2^* = 2H^*$	−54
12	$C_2H_2 + * = CHCH^*$	−115
13	$C_2H_4 + * = CH_2CH_2^*$	52

Reference state: $C_2H_2(gas) + 2H_2(gas) + Pt(1\,1\,1)$-$CCH_3$ for steps 1–10, and Pt(1 1 1)-CCH_3 plus gaseous adsorbate for steps 11–13.

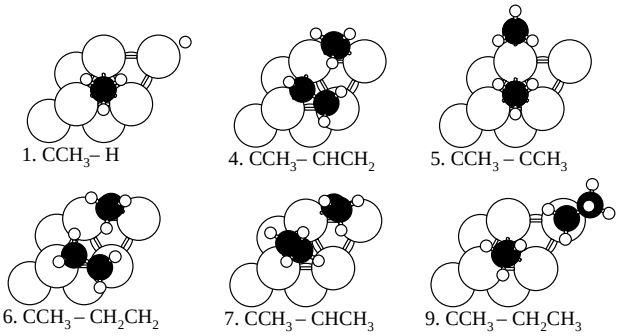

Fig. 6. Geometries of stable species on ethylidyne CCH_3-covered surface. Numbers correspond to entries in Table 4. Entry 8 is not shown: CCH_3 plus gas-phase ethylene. Entries 2 and 3 are shown, correspondingly, in Fig. 3(6) and (5).

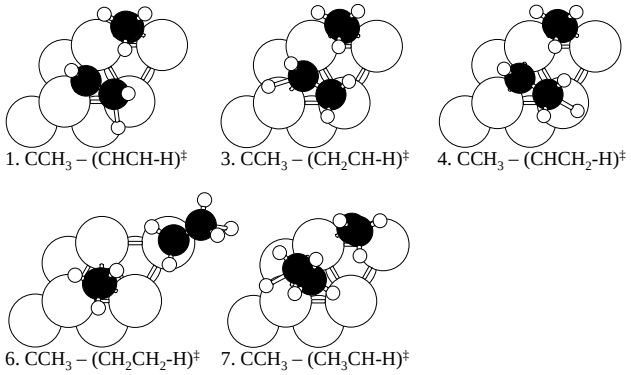

Fig. 7. Geometries of transition states on Pt(1 1 1)-CCH_3. Numbers correspond to reactions in Table 2. Reactions 2 and 5 in Table 2, CCH_2 and CCH_3 hydrogenation, were not evaluated.

The most favorable location for a hydrogen atom in the presence of ethylidyne is an fcc site, as shown in Fig. 6(1). A configuration with an H atom in a neighboring hcp site is less favorable by 11 kJ/mol. The arrangement in Fig. 6(1) corresponds to the energy change for dissociative adsorption of H_2 on the ethylidyne-covered surface of −54 kJ/mol (entry 11 in Table 4), and this value is lower by 19 kJ/mol than the adsorption energy on the vinylidene-covered surface and by 32 kJ/mol lower than that on the clean surface. This result is consistent with TPD evidence that the presence of an ethylidyne monolayer significantly weakens hydrogen adsorption on Pt(1 1 1) under UHV conditions [62]. Substituting vinylidene with ethylidyne generally stabilizes the additional hydrocarbon in the unit cell. For example, acetylene is more stable by 39 kJ/mol with ethylidyne than with vinylidene.

The configuration with two ethylidyne species in Fig. 6(5) is the most stable arrangement for all high-coverage calculations for this overall stoichiometry, i.e., four carbon and six hydrogen atoms in the same unit cell. A similar configuration with both ethylidynes in fcc sites is less favorable by about 40 kJ/mol.

Similar to the vinylidene-covered surface, a distorted di-σ-species in Fig. 6(6) is the most stable ethylene adsorption mode, corresponding to an ethylene adsorption energy of 52 kJ/mol (endothermic reaction due to ethylidyne destabilization), entry 13 in Table 4. This result is in agreement with experimental evidence that a saturated layer of ethylidyne prevents ethylene adsorption on Pt(1 1 1) [7,62,63]. The geometries of $CHCH_3$ and CH_2CH_3 on clean, vinylidene- and ethylidyne-covered surfaces are similar. The CH_2CH_3 geometry is least affected by high coverage because these species preferentially occupy an atop site and can minimize lateral repulsive interactions due to the unhindered methyl group rotation.

8. Transition states on Pt(1 1 1)-CCH_3

A summary of transition state energetics for Pt-CCH_3 is provided in the third column of Table 2, and the corresponding geometries are shown in Fig. 7. The transition state structures are similar to the structures on the vinylidene-covered surface in Fig. 4. Accordingly, the energy values for the ethylidyne- and vinylidene-covered surfaces are similar (Tables 3 and 4). Specifically, compared to the results on the clean surface, both potential energy surfaces are shifted up by about 170 kJ/mol. Additionally, the barrier for ethylene formation is higher and the barrier for ethylene hydrogenation is lower (reactions 3 and 6 in Table 2). Therefore, these trends do not appear to depend on the type of a spectator species, and they can be characterized as high-coverage effects. These effects can be summarized as follows: hydrocarbon species and hydrogen atoms are destabilized by as much as 150 and 30 kJ/mol, respectively. As expected, the destabilization effect is higher for multiply-bonded species, so that the reaction energy diagrams at high and low coverage become closer as more saturated species are formed during hydrogenation, as seen in Fig. 5. In addition, activation energies are not affected, unless the spatial formation of a transition state is hindered or a reactant is significantly distorted. When the spatial formation of the transition state is hindered, as in the case of ethylene formation, the activation energy can increase by as much as 44 kJ/mol (reaction 3 in Table 2b). On the other hand, the activation barrier can decrease by as much as 34 kJ/mol, as in the case of ethylene hydrogenation (reaction 6 in Table 2b), when the reacting hydrocarbon is distorted and thus destabilized.

9. Disproportionation reactions with a CCH_2–CCH_3 transition

The role of carbonaceous surface deposits in hydrogenation reactions has been investigated by various experimental techniques. For example, although the rates of H–D exchange reactions for ethylidyne species on Pt(1 1 1) were found to be orders of magnitude lower than the rate

Table 5
Energetics of transition states for hydrogen disproportionation reactions with a CCH_2–CCH_3 transition (kJ/mol)

	Reaction	Pt	
		E_a	ΔE
1	$CCH_2 + CHCH_2 = CCH_3 + CHCH$	53	−59
2	$CCH_2 + CH_2CH_2 = CCH_3 + CHCH_2$	45	−105
3	$CCH_2 + CHCH_3 = CCH_3 + CHCH_2$	29	−127
4	$CCH_2 + CH_2CH_3 = CCH_3 + CH_2CH_2$	61	−26
5	$CCH_2 + CH_2CH_3 = CCH_3 + CHCH_3$	144	−12

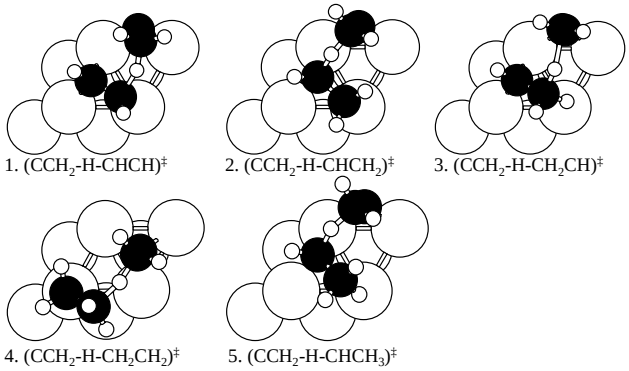

Fig. 8. Geometries of transition states for hydrogen disproportionation reactions with a CCH_2 to CCH_3 transition. Numbers correspond to entries in Table 5.

of ethylene hydrogenation [1,7,64–66], disproportionation reactions were shown to be important during thermal evolution of acetylene and ethylene from Pt(1 1 1) [32,34,58,67]. Ethylidyne was proposed to act as a hydrogen transfer agent through the formation of $CHCH_3$ species [7,58]. Furthermore, kinetic, TPD, and surface titration studies using transient conditions and isotope labels on single-crystal and supported Pt and Pd have been interpreted in terms of a direct participation of spectator species in hydrogenation [5,62,68–70]. This experimental evidence led to the proposed description of spectator species as "a nonselective poison which blocks platinum surface sites" [70], with the most important reaction properties of these spectators being their "ability to store and exchange hydrogen with reacting surface species and to provide desorption sites for product molecules" [70]. We, thus, evaluated hydrogen disproportionation reactions between a spectator species and a neighboring hydrocarbon species.

Transition states for hydrogen transfer reactions were obtained using vinylidene geometries of Fig. 3 by bringing the vinylidene close to a neighboring hydrocarbon in such a way that the upper carbon of the vinylidene was 1.3 Å away from the reacting hydrogen. Then, the C–H distance for the neighboring hydrocarbon was constrained, and the whole structure was allowed to optimize. The constrained C–H distance was taken as the reaction coordinate. This distance is about 1.3–1.4 Å for the identified transition states, which is smaller than the values of 1.5–1.8 Å for reactions with surface hydrogen. The energetics of hydrogen disproportionation reactions are summarized in Table 5 and the corresponding geometries are shown in Fig. 8. In each reaction, it is energetically favorable for vinylidene to extract a hydrogen atom from the neighboring hydrocarbon, forming ethylidyne. The estimates for the activation barriers vary from 29 to 144 kJ/mol, Table 5. These disproportionation reactions can be competitive pathways, since the energetic penalty for bringing a hydrogen atom into the unit cell at high hydrocarbon coverage is about 50–70 kJ/mol, and, correspondingly, the intrinsic activation barriers for direct hydrogenation are at least 67 kJ/mol for our model surfaces (Table 2b).

A possible modification of the reaction mechanism in which hydrogen disproportionation reactions provide a lower energy pathway is illustrated in Fig. 9. The lower energy sequence of steps is shown with arrows. This figure expands a part of the acetylene hydrogenation energy diagram in Fig. 5 for the Pt-CCH_2 surface, where ethylene is hydrogenated through surface hydrogen only. The diagram in Fig. 5 suggests that ethylene readily desorbs from the Pt-CCH_2 surface and that its subsequent hydrogenation is unlikely. However, if disproportionation reactions are taken into account, gas-phase ethylene can be stabilized on the vinylidene-covered surface by donating hydrogen and forming $CHCH_2$ and CCH_3 species (Fig. 8(2)), with an overall energy change of −49 kJ/mol. The $CHCH_2$ formed in this step can then be hydrogenated to ethylene in the presence of ethylidyne (reaction 3 in Table 2). It is then more energetically favorable for ethylene to abstract a hydrogen from Pt-CCH_3 to form C_2H_5 (barrier of 87 kJ/mol, Fig. 8(4)) than to react with a surface hydrogen atom (barrier of 106 kJ/mol, Fig. 7(6)). Thus, the net reaction in Fig. 9 is

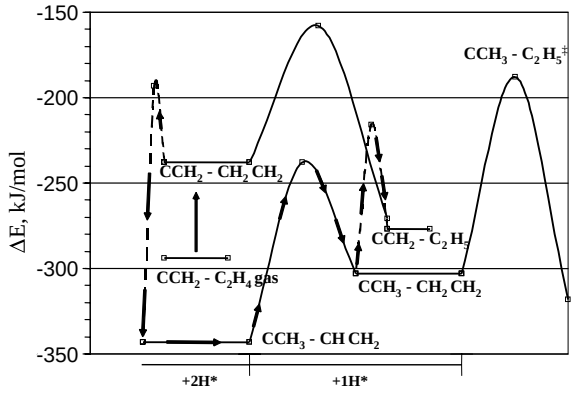

Fig. 9. A modified reaction mechanism for C_2H_4 hydrogenation where hydrogen disproportionation reactions with a vinylidene to ethylidyne transition (denoted by dashed lines) provide a lower-energy pathway. The original diagram with hydrogenation through surface hydrogen only is shown in Fig. 5. Reference state: C_2H_2(gas) + $2H_2$(gas) + Pt(1 1 1)-CCH_2.

ethylene hydrogenation to C_2H_5 in the presence of vinylidene, involving an intermediate transition of vinylidene to ethylidyne.

10. Influence of high coverage on selectivity to ethylene

The results from DFT calculations suggest that there are three main hydrocarbon coverage effects with respect to the selectivity to ethylene formation. First, the presence of spectator species destabilizes reactive species, as illustrated in Fig. 5. At high coverage, ethylene desorption becomes more competitive than further hydrogenation, and, accordingly, ethylene re-adsorption becomes less favorable, leading to higher ethylene selectivity. This result is in agreement with the reported effects of "carbonaceous deposits" on the reaction selectivity over silica-supported Pt and Pd catalysts [71] and reported kinetic data for many other transition metals [11,12,71].

The second effect relates to changes in activity because of unequal destabilization of reactive hydrocarbon species and because certain reaction pathways become unfavorable. This role of the spectator species can explain differences in apparent activation energies for hydrogenation reactions under UHV conditions, when no spectators are present, and under typical conditions for hydrogenation reactions. Specifically, the calculations indicate that adsorbed ethylene is affected more than the $CHCH_3$ species, and the formation of the latter species becomes more favorable at high coverage, as shown in Fig. 5 and Table 2b. The formation of $CHCH_3$ species provides a direct route for conversion of acetylene to ethane without passing through ethylene. Therefore, the competition between the alternative $CHCH_2$ hydrogenation products can influence the selectivity to ethylene. Ethane formation from $CHCH_3$ species, an example of "mechanistic" selectivity [11,12], is consistent with acetylene hydrogenation studies in the presence of ^{14}C ethylene over Pt/SiO_2, which showed that re-adsorbed ethylene did not contribute significantly to ethane production under conditions of hydrocarbon conversion below 50% and selectivity to ethylene below 30% [69]. The conjecture of competing $CHCH_2$ hydrogenation steps is also consistent with the experimental observation that the selectivity over Pt increases with temperature [11]: at higher temperatures, the difference in activation energies would be less kinetically significant, and, therefore, the ethylene production step would be more competitive with the $CHCH_3$ formation step. The third effect is the ability of spectator species to exchange hydrogen with reactive species and provide lower energy reaction pathways. These additional reactions, which are distinct from steps involving surface hydrogen, may, for example, contribute to lower selectivity, since gas-phase ethylene can be stabilized on the surface by vinylidene and then react further to produce ethane, as shown in Fig. 9. For a Pt/SiO_2 catalyst, ethylene re-adsorption and further hydrogenation to ethane at high coverage have been demonstrated with ^{14}C experiments [69].

11. Conclusions

Results of DFT calculations for acetylene hydrogenation on clean, vinylidene-covered (0.25 ML) and ethylidyne-covered (0.25 ML) Pt(1 1 1) surfaces confirm that vinylidene CCH_2 and ethylidyne CCH_3 are important spectator species. The activation barrier for vinylidene hydrogenation in the presence of acetylene is higher than that for acetylene in the same configuration. In addition, vinylidene preferentially forms unreactive ethylidyne species on hydrogenation. The activation energy estimate for ethylidyne hydrogenation is 30–80 kJ/mol higher than the calculated barriers for all other considered direct hydrogenation steps.

Energetic trends due to high coverage are similar for both vinylidene- and ethylidyne-covered surfaces. These trends can be characterized by three main effects. The first effect is destabilization of reactive species: hydrocarbon species and hydrogen atoms are destabilized by as much as 150 and 30 kJ/mol, respectively, compared to the clean surface. Unsaturated, multiply-bonded species are destabilized more than species forming fewer bonds with the surface. This destabilization effect favors desorption of product species.

The second effect relates to changes in activity because of unequal destabilization of reactive hydrocarbon species and because of spatial hindrance for certain reaction pathways. For example, the lower-energy reaction pathway for ethylene formation, depicted in Fig. 2a, becomes unfavorable at high coverage, and the activation energy for this step increases by 44 kJ/mol. Fig. 5 shows that the relative propensity of $CHCH_2$ species for forming either $CHCH_3$ or CH_2CH_2 is reversed at high coverage because of spatial hindrance. Another example is relatively higher destabilization of adsorbed CH_2CH_2 compared to $CHCH_3$. This effect leads to lower activation energies for ethylene hydrogenation. As shown in Fig. 5, this activation energy is lower by 34 kJ/mol in the presence of vinylidene.

The third effect relates to the ability of hydrocarbon species to exchange hydrogen atoms, undergo disproportionation, at high surface coverage. In this study, disproportionation reactions with a vinylidene to ethylidyne transition were considered. Depending on the surface species, a hydrocarbon species can donate a hydrogen atom to vinylidene to produce ethylidyne or can abstract a hydrogen from ethylidyne to produce vinylidene. Therefore, spectator species can serve as a hydrogen reservoir, changing from hydrogen-poor to hydrogen-rich depending on the reaction conditions. The disproportionation reactions can provide lower-energy alternatives to reaction steps with surface hydrogen, and, thus, influence both activity and selectivity. This effect is illustrated in Fig. 9, where the pathway for ethylene re-adsorption and hydrogenation to C_2H_5 becomes more favorable when disproportionation reactions with

a vinylidene to ethylidyne transition are included in the mechanism.

Acknowledgements

Acknowledgment is made to the Donors of the Petroleum Research Fund, administered by the American Chemical Society, for support of this research.

References

[1] T.P. Beebe, J.T. Yates, J. Am. Chem. Soc. 108 (1986) 663.
[2] P.S. Cremer, X.C. Su, Y.R. Shen, G.A. Somorjai, J. Am. Chem. Soc. 118 (1996) 2942.
[3] J.E. Rekoske, R.D. Cortright, S.A. Goddard, S.B. Sharma, J.A. Dumesic, J. Phys. Chem. 96 (1992) 1880.
[4] S. Azad, M. Kaltchev, D. Stacchiola, G. Wu, W.T. Tysoe, J. Phys. Chem. B 104 (2000) 3107.
[5] S.M. Davis, F. Zaera, B.E. Gordon, G.A. Somorjai, J. Catal. 92 (1985) 240.
[6] G.A. Somorjai, G. Rupprechter, J. Phys. Chem. B 103 (1999) 1623.
[7] F. Zaera, G.A. Somorjai, J. Am. Chem. Soc. 106 (1984) 2288.
[8] R.M. Watwe, R.D. Cortright, J.K. Norskov, J.A. Dumesic, J. Phys. Chem. B 104 (2000) 2299.
[9] S.G. Podkolzin, R.M. Watwe, Q. Yan, J.J. de Pablo, J.A. Dumesic, J. Phys. Chem. B 105 (2001) 8550.
[10] R. Alcala, M. Mavrikakis, J.A. Dumesic, J. Catal. 218 (2003) 178.
[11] G.C. Bond, P.B. Wells, in: D.D. Eley, H. Pines, P.B. Weisz (Eds.), Advances in Catalysis and Related Subjects, vol. 15, Academic Press, New York, 1964, p. 92.
[12] G. Webb, in: C.H. Banford, C.F.H. Tipper (Eds.), Comprehensive Chemical Kinetics, vol. 20, Elsevier, Amsterdam, 1978, p. 1.
[13] A.N.R. Bos, K.R. Westerterp, Chem. Eng. Process. 32 (1993) 1.
[14] F. Zaera, T.V.W. Janssens, H. Öfner, Surf. Sci. 368 (1996) 371.
[15] F. Zaera, Int. Rev. Phys. Chem. 21 (2002) 433.
[16] F. Zaera, Mol. Phys. 100 (2002) 3065.
[17] F. Zaera, Appl. Catal. A 229 (2002) 75.
[18] B. Hammer, L.B. Hansen, J.K. Norskov, Phys. Rev. B 59 (1999) 7413.
[19] H.Y. Afeefy, J.F. Liebman, S.E. Stein, in: P.J. Linstrom, W.G. Mallard (Eds.), NIST Chemistry WebBook, NIST Standard Reference Database No. 69, National Institute of Standards and Technology, Gaithersburg, 2003.
[20] G.J. Hutchings, J.K. Bartley, C. Rhodes, S.H. Taylor, R.P.K. Wells, D.J. Willock, in: I.T. Horvath (Ed.), Encyclopedia of Catalysis, vol. 4, Wiley, Hoboken, 2004, p. 671.
[21] J. Kua, W.A. Goddard III, J. Phys. Chem. B 102 (1998) 9492.
[22] B.E. Spiewak, R.D. Cortright, J.A. Dumesic, J. Catal. 176 (1998) 405.
[23] R.M. Watwe, B.E. Spiewak, R.D. Cortright, J.A. Dumesic, J. Catal. 180 (1998) 184.
[24] J.W. Medlin, M.D. Allendorf, J. Phys. Chem. B 107 (2003) 217.
[25] T. Felter, W. Weinberg, Surf. Sci. 103 (1981) 265.
[26] H. Ibach, S. Lehwald, J. Vac. Sci. Technol. A 15 (1978) 407.
[27] C.J. Baddeley, A.F. Lee, R.M. Lambert, T. Giessel, O. Schaff, V. Fernandez, K.M. Schindler, A. Theobald, C.J. Hirschmugl, R. Lindsay, A.M. Bradshaw, D.P. Woodruff, Surf. Sci. 400 (1998) 166.
[28] A. Clotet, G. Pacchioni, Surf. Sci. 346 (1996) 91.
[29] M.R. Albert, L.G. Sneddon, W. Eberhardt, F. Greuter, T. Gustafsson, E.W. Plummer, Surf. Sci. 120 (1982) 19.
[30] L.L. Kesmodel, R.C. Baetzold, G.A. Somorjai, Surf. Sci. 66 (1977) 299.
[31] J.E. Demuth, Surf. Sci. 80 (1979) 367.
[32] N.R. Avery, Langmuir 4 (1988) 445.
[33] P. K Wang, C.P. Slichter, J.H. Sinfelt, Phys. Rev. Lett. 53 (1984) 82.
[34] P.S. Cremer, X.C. Su, Y.R. Shen, G.A. Somorjai, J. Phys. Chem. B 101 (1997) 6474.
[35] D.B. Kang, A.B. Anderson, Surf. Sci. 155 (1985) 639.
[36] V. Maurice, C. Minot, Langmuir 5 (1989) 734.
[37] J.F. Paul, P. Sautet, J. Phys. Chem. 98 (1994) 10906.
[38] Q. Ge, D.A. King, J. Chem. Phys. 110 (1999) 4699.
[39] T. Miura, H. Kobayashi, K. Domen, J. Phys. Chem. B 104 (2000) 6809.
[40] G.W. Watson, R.P.K. Wells, D.J. Willock, G.J. Hutchings, J. Phys. Chem. B 104 (2000) 6439.
[41] J.Y. Shen, J.M. Hill, R.M. Watwe, B.E. Spiewak, J.A. Dumesic, J. Phys. Chem. B 103 (1999) 3923.
[42] G. Szulczewski, R.J. Levis, J. Am. Chem. Soc. 118 (1996) 3521.
[43] A. Stuck, C.E. Wartnaby, Y.Y. Yeo, D.A. King, Phys. Rev. Lett. 74 (1995) 578.
[44] J. Kubota, S. Ichihara, J.N. Kondo, K. Domen, C. Hirose, Surf. Sci. 358 (1996) 634.
[45] D. Velic, R.J. Levis, J. Chem. Phys. 104 (1996) 9629.
[46] H. Öfner, F. Zaera, J. Am. Chem. Soc. 124 (2002) 10982.
[47] Y.Y. Yeo, A. Stuck, C.E. Wartnaby, D.A. King, Chem. Phys. Lett. 259 (1996) 28.
[48] S. Palfi, W. Lisowski, M. Smutek, S. Cerny, J. Catal. 88 (1984) 300.
[49] M.A. Natal-Santiago, S.G. Podkolzin, R.D. Cortright, J.A. Dumesic, Catal. Lett. 45 (1997) 155.
[50] T.V.W. Janssens, F. Zaera, J. Phys. Chem. 100 (1996) 14118.
[51] F. Zaera, C.R. French, J. Am. Chem. Soc. 121 (1999) 2236.
[52] H. Öfner, F. Zaera, J. Phys. Chem. B 101 (1997) 396.
[53] G.A. Somorjai, F. Zaera, J. Phys. Chem. 86 (1982) 3070.
[54] M. Neurock, R.A. van Santen, J. Phys. Chem. B 104 (2000) 11127.
[55] F. Zaera, J. Phys. Chem. 94 (1990) 8350.
[56] F. Zaera, Surf. Sci. 219 (1989) 453.
[57] F. Zaera, J. Am. Chem. Soc. 111 (1989) 4240.
[58] F. Zaera, Langmuir 12 (1996) 88.
[59] R. Doll, C.A. Gerken, M.A. VanHove, G.A. Somorjai, Surf. Sci. 374 (1997) 151.
[60] C.A. Klug, C.P. Slichter, J.H. Sinfelt, J. Phys. Chem. 95 (1991) 2119.
[61] P.A. Sheth, M. Neurock, C.M. Smith, J. Phys. Chem. B 107 (2003) 2009.
[62] D. Godbey, F. Zaera, R. Yeates, G.A. Somorjai, Surf. Sci. 167 (1986) 150.
[63] A. Wieckowski, S.D. Rosasco, G.N. Salaita, A. Hubbard, B.E. Bent, F. Zaera, G.A. Somorjai, J. Am. Chem. Soc. 107 (1985) 5910.
[64] M. Salmeron, G.A. Somorjai, J. Phys. Chem. 86 (1982) 341.
[65] B.E. Koel, B.E. Bent, G.A. Somorjai, Surf. Sci. 146 (1984) 211.
[66] T.V.W. Janssens, F. Zaera, Surf. Sci. 344 (1995) 77.
[67] D. Godbey, F. Zaera, R. Yeates, G.A. Somorjai, Surf. Sci. 167 (1986) 150.
[68] A.S. Al-Ammar, G. Webb, J. Chem. Soc., Faraday Trans. 74 (1978) 195.
[69] E.A. Arafa, G. Webb, Catal. Today 17 (1993) 411.
[70] S.M. Davis, F. Zaera, G.A. Somorjai, J. Catal. 77 (1982) 439.
[71] J. Houzvicka, R. Pestman, V. Ponec, Catal. Lett. 30 (1995) 289.